THE JOURNAL OF BIOLOGICAL CHEMISTRY
Vol. 279, No. 37, Issue of September 10, pp. 38755–38761, 2004
Printed in U.S.A.

Solution Structure and Antibody Binding Studies of the Envelope Protein Domain III from the New York Strain of West Nile Virus*

Received for publication, March 3, 2004, and in revised form, June 4, 2004
Published, JBC Papers in Press, June 9, 2004, DOI 10.1074/jbc.M402385200

David E. Volk‡§, David W. C. Beasley¶‖, Deborah A. Kallick‡§, Michael R. Holbrook¶‖, Alan D. T. Barrett¶‖, and David G. Gorenstein‡§**

From the ‡Sealy Center for Structural Biology, ¶the Sealy Center for Vaccine Development, and the Departments of §Human Biological Chemistry and Genetics and ‖Pathology, University of Texas Medical Branch, Galveston,Texas 77555-1147

The solution structure of domain III from the New York West Nile virus strain 385-99 (WN-rED3) has been determined by NMR methods. The West Nile domain III structure is a β-barrel structure formed from seven anti-parallel β-strands in two β-sheets. One anti-parallel β-sheet consists of β-strands β1 (Phe^{299}-Asp^{307}), β2 (Val^{313}-Tyr^{319}), β4 (Arg^{354}-Leu^{355}), and β5 (Lys^{370}-Glu^{376}) arranged so that β2 is flanked on either side by β1 and β5. The short β4 flanks the end of the remaining side of β5. The remaining anti-parallel β-sheet is formed from strands β3 (Ile^{340}-Val^{343}), β6 (Gly^{380}-Arg^{388}), and β7 (Gln^{391}-Lys^{399}) arranged with β6 at the center. Residues implicated in antigenic differences between different West Nile virus strains (and other flaviviruses) and neutralization are located on the outer surface of the protein. Characterization of the binding of monoclonal antibodies to WN-rED3 mutants, which were identified through neutralization escape experiments, indicate that antibody neutralization directly correlates with binding affinities. These studies provide an insight into theoretical virus-receptor interaction points, structure of immunogenic determinants, and potential targets for antiviral agents against West Nile virus and highlight differences between West Nile virus and other flavivirus structures that may represent critical determinants of virulence.

In 2002, the mosquito-borne West Nile virus (WNV)[1] (family *Flaviviridae*, genus *Flavivirus*) was responsible for the largest outbreak of arthropod-borne encephalitis recorded in the Western hemisphere. In that year, 4156 human infections and 284 deaths were reported in the United States (1). In 2003, the WNV epidemic continued with large numbers of human and animal disease across North America, and it was detected for the first time in Mexico and Central America (*e.g.* Refs. 2–4). The objective of this study was to solve the solution structure for the putative envelope (E) protein, the receptor-binding domain of WNV with the long term goal of using these findings for the development of structure-based vaccines or antiviral agents. Currently, there are no approved vaccines for WNV or therapeutic treatments for West Nile encephalitis.

The flaviviruses are small, enveloped, positive-sense RNA viruses that are transmitted primarily by either mosquitoes or ticks. The translation of the single open reading frame within the viral genome, followed by co- and posttranslational cleavage, results in ten viral proteins, three structural proteins (core, membrane, and E) and seven non-structural proteins. The non-structural proteins are involved in viral replication and pathogenesis, whereas the three structural proteins are assembled into the mature virus particle.

The E protein is the major surface protein of the flavivirus virions. The E protein is also the primary immunogen and plays a central role in virus attachment and entry to cells via membrane fusion. The x-ray crystallographic structures of the E protein ectodomains of both the tick-borne central European encephalitis virus (5) and the mosquito-borne dengue-2 virus (6) have been solved. Both proteins contain three distinct structural domains (domains I, II, and III) that correspond to previously characterized antigenic domains (7). Domain III (D3) of the E protein was initially proposed as the likely receptor-binding domain of the flaviviruses because of its structural characteristics. These include an IgC-like fold and a four-amino-acid loop that contains an RGD integrin-binding motif in several of the mosquito-borne flaviviruses (5). More recent studies have shown that D3 is directly associated with binding of dengue-2 virus (DEN2V) (8), WNV, and the tick-borne Langat virus[2] to cells. Domain 3 of WNV (WN-rED3) has also been shown to contain epitopes recognized by virus-neutralizing monoclonal antibodies (9). X-ray crystallography (5, 6) and cryo-electron microscopy studies (6, 10, 11) of the mosquito-borne WNV, DEN2V, and yellow fever virus have found that the E protein is arranged in dimeric form on the virus surface. Located at the 5- and 3-fold axes of symmetry, D3 projects slightly above the virion surface, allowing access to potential receptor molecules and antibodies. The 5-fold axis is arranged such that there is a "pore" between the D3 molecules. When the

* This work was supported by Grants U01 A1054827 from the NIAID, National Institutes of Health, P42296LS0000 from the Defense Advanced Research Projects Agency, U90CCU618754 from the Centers for Disease Control, DAAD13-02-C-0079 and DAAD17-01-D-0001 from Defense Threat Reduction Agency, 004952-0038-2003 from the State of Texas Advanced Technology Program, and fellowships from The James W. McLaughlin Fellowship Fund (to D. W. C. B.) and T32 AI007536-06 from the National Institutes of Health (to M. R. H.). The costs of publication of this article were defrayed in part by the payment of page charges. This article must therefore be hereby marked "*advertisement*" in accordance with 18 U.S.C. Section 1734 solely to indicate this fact.

The atomic coordinates and structure factors (code 1S6N) have been deposited in the Protein Data Bank, Research Collaboratory for Structural Bioinformatics, Rutgers University, New Brunswick, NJ (http://www.rcsb.org/).

** To whom correspondence should be addressed: Route 1147, University of Texas Medical Branch, Galveston, TX 77555-1147. Tel.: 409-747-6800; Fax: 409-747-6850; E-mail: david@nmr.utmb.edu.

[1] The abbreviations used are: WNV, West Nile virus; E, envelope protein; D3, domain III; WN-rED3, West Nile recombinant envelope protein domain III; JEV, Japanese encephalitis virus; DENV, dengue virus; MAb, monoclonal antibody; NOE, nuclear Overhauser effect; TOCSY, total correlation spectroscopy; r.m.s.d., root mean square distance.

[2] M. R. Holbrook, unpublished results.

flaviviruses bind to a target cell, they are internalized into an endosome that is acidified. The drop in pH causes a dramatic conformational shift in the E protein that exposes the viral fusion peptide (12), allows the endosomal and viral membranes to fuse, and provides for the release of the viral RNA into the cell cytoplasm.

The role of the flavivirus E-D3 in virus-receptor binding makes it an attractive target for the development of vaccines, antiviral agents, and/or diagnostic antigens. The solution structure of the WN-rED3 described here, along with that of the closely related Japanese encephalitis virus (JEV) (13), provides fundamental knowledge for the development of structure-based vaccines and antiviral agents to protect against and treat diseases caused by WNV and related flaviviruses.

EXPERIMENTAL PROCEDURES

Protein Expression and Purification—Uniformly ^{13}C,^{15}N-labeled recombinant WN-rED3 from neuroinvasive lineage 1 West Nile virus strain 385-99 was overexpressed as a maltose-binding protein fusion using the pMAL-c2X vector as described previously (9), and the 115-residue WN-rED3 was purified using size-exclusion chromatography. Residues Leu^{6}–Ser^{112} of the 115-residue protein align with residues Leu^{297}–Ser^{403} of the 385-99 envelope protein. Residues 1–5 and 113–115 were included in this construct to increase protein solubility. In addition, the QuikChange XL site-directed mutagenesis kit (Stratagene) was used to derive E-D3 fusion proteins encoding mutations at K307R or T330I. These mutations had been shown previously to affect neutralization of WNV by monoclonal antibodies (9).

Monoclonal Antibody Neutralization and Binding Assays—Neutralization assays with four WNV-specific neutralizing antibodies, designated 7H2, 5H10, 5C5, and 3A3 (Bioreliance), against WNV NY99 and variants monoclonal antibody $(MAb)^{R}$-5H10 and -5C5 were performed with MAbs at 10 nM concentration as described elsewhere (9). The binding characteristics of the four MAbs to recombinant NY99 E-D3 and the K307R and T330I mutant E-D3 MBP fusion proteins were investigated using a titration enzyme-linked immunosorbent assay similar to that described by Lin and Wu (15). Briefly, wells of 96-well enzyme-linked immunosorbent assay plates were coated overnight at 4 °C with 60 ng/well purified fusion protein (equivalent to ~11 ng of E-D3). After blocking in phosphate-buffered saline containing 0.5% Tween 20 (phosphate-buffered saline-Tween) and 3% bovine serum albumin, serial dilutions of MAbs from 100 to 0.003 nM were dispensed into replicate wells and incubated at room temperature (25 °C) for 60 min. After washing three times with phosphate-buffered saline-Tween, horseradish peroxidase-labeled anti-mouse Ig antiserum was added to each well, and the plates were incubated again, prior to washing and addition of TMB substrate. Color development was for 15 min, after which the reactions were stopped with 3 M HCl, and absorbance values were read at 450 nm. Binding curves and K_d values were determined using Sigmaplot (SPSS Inc., Chicago, IL).

NMR Spectroscopy and Generation of Restraints—The NMR sample contained 0.7 mM protein in 50 mM K_2HPO_4 (pH 6.8), 100 mM NaCl, 10 mM NaN_3, and 0.1 mM EDTA in 90% H_2O, 10% D_2O. All NMR experiments were acquired on Varian UnityPlus 600 or 750 MHz spectrometers at 25 °C. Sequence-specific chemical shifts for the backbone atoms were obtained from three-dimensional HNCA, HNCACB (16), and HNCO (17) experiments. The backbone assignments were verified through sequential NH-NH and NH-Hα nuclear Overhauser effects (NOEs) in a 150-ms mixing time ^{15}N-edited three-dimensional nuclear Overhauser enhancement spectroscopy-heteronuclear single quantum correlation spectrum (18). Side chain chemical shifts were obtained from three-dimensional H(CCO)NH-total correlation spectroscopy (TOCSY) (19), CC(CO)NH-TOCSY, TOCSY-HSQC{^{1}H,^{15}N}, and HCCH-TOCSY (20) experiments. The CC(CO)NH-TOCSY experiment also aided in the assignments of the C-α and C-β carbons in cases of degeneracy in the HNCACB experiment and in the assignments of the Asn and Gln side chain amide groups. Aromatic chemical shifts were assigned based on a CT-^{1}H,^{13}C-HSQC spectrum, NOE data, and a HCCH-TOCSY spectrum with the carbon frequency centered on the aromatic carbons. Spectra were processed using VNMR v6.1b (Varian, Inc.) or Felix98 (MSI, Inc.) software.

The program SANE (21) was used to facilitate the assignment of some NOE cross-peaks and for the generation of restraints. Within the SANE program, chemical shift, distance cutoff, and secondary structure filters were used. The NOE restraints were separated into three bins based on their volumes, and the upper distance limits of the restraints were set to 2.8, 3.8, and 5.5 Å. The 1239 NOE-based restraints (see Table I) consist of 299 intra-residue, 433 sequential, 104 medium range, and 403 long range NOE restraints.

The program TALOS (22) was used to derive ϕ/ψ angle restraints. After two rounds of preliminary molecular dynamics calculations, those dihedral angles inconsistent with the NOE data were removed or changed to the ϕ/ψ angle exhibited by fewer of the proteins in the TALOS data bank. Additionally, ω dihedral angle and chiral angle restraints were also used.

Restrained Molecular Dynamics Calculations—One hundred random structures were generated by annealing the protein at 1500 K, obtaining the coordinates every 5 ps, and minimizing the structures obtained. During the annealing process, chiral restraints were applied to maintain the correct chirality for all amino acids. Each of these structures was then subjected to 15 ps of restrained molecular dynamics with the following protocol. During the first 5 ps, the restraints were increased linearly from 0 to 20 kcal/mol $Å^2$, the non-bonded interactions (electrostatic, van der Waals, and hydrogen bonding terms) were set to 10% of their normal values, and the temperature was increased from 100 to 700 K. During the next 5 ps the non-bonded interactions were increased linearly from 10 to 100%, while the temperature remained set to 700 K. During the final 5 ps, the temperature was decreased linearly from 700 to 100 K while the full force constants of the restraints and the non-bonded interactions were applied. Each of the structures obtained was subsequently subjected to 2000 steps of energy minimization. Fifteen structures with low restraint penalties were then chosen for the structural ensemble. All calculations were done with the SANDER module within AMBER6 (23). Structures were visualized with MIDAS (23) or MOLMOL (24), which was used to generate Figs. 1 and 3. Atomic coordinates for fifteen structures have been deposited with the Protein Data Bank (PDB ID 1S6N) and the chemical shifts have been deposited at the BioMagResBank under accession code 6046 (25).

RESULTS

Quality of the Final Structure—The 15 final structures in the ensemble (Fig. 1) had low molecular and restraint energy penalties. The final structures had 6 ± 2 distance restraint violations over 0.3 Å, and 8 ± 1 dihedral angle violations over 20° (Table I). The dihedral angle restraints used were very restrictive in angular space; the tightest restraint was ±3°, and 75% of the dihedral angles were restricted to less than ±20° from the target angle. Therefore, a violation cutoff of 20° is reasonable for the restraints used. The r.m.s.d. restraint error was 0.0156 ± 0.0017 Å, and the r.m.s.d. angle restraint error was 1.60 ± 0.06°. The structural ensemble has an average pairwise atomic r.m.s.d. of 0.65 ± 0.12 Å for the backbone atoms and 0.98 ± 0.17 Å for all heavy atoms for residues 13–108 of the protein.

The program PROCHECK (14) was used to analyze the quality of the ensemble of structures. Ramachandran analysis of the non-glycine, non-proline residues indicated 98% of the residues are in the two most favored regions of the Ramachandran plot. Specifically, 76.8% are in the most favored region, 21.2% are in the additionally allowed region, 0.7% are in the generously allowed region, and 1.2% are in the disallowed region. Ser^{400} is in the disallowed region in two of the fifteen structures, whereas Lys^{307}, which is near the disulfide bond between Cys^{305} and Cys^{336}, is in the disallowed region in every structure.

Interaction of WNV-specific Neutralizing Monoclonal Antibodies with E-D3—Previously we have described the preliminary determination of *in vitro* neutralization characteristics of four WNV-specific MAbs that bound to WNV E-D3 (9). To better characterize the interactions of these MAbs with E-D3 and the relationship between MAb binding and virus neutralization we titrated the specific binding of each MAb with the WN-rED3 MPB fusion protein in enzyme-linked immunosorbent assays. Based on these titrations (Fig. 2*A*), the calculated K_d values for each MAb were comparable, ranging between 0.1 and 0.2 nM. Interestingly, the maximal binding of MAb 7H2 was 20% higher than those of the other MAbs (Fig. 2), which

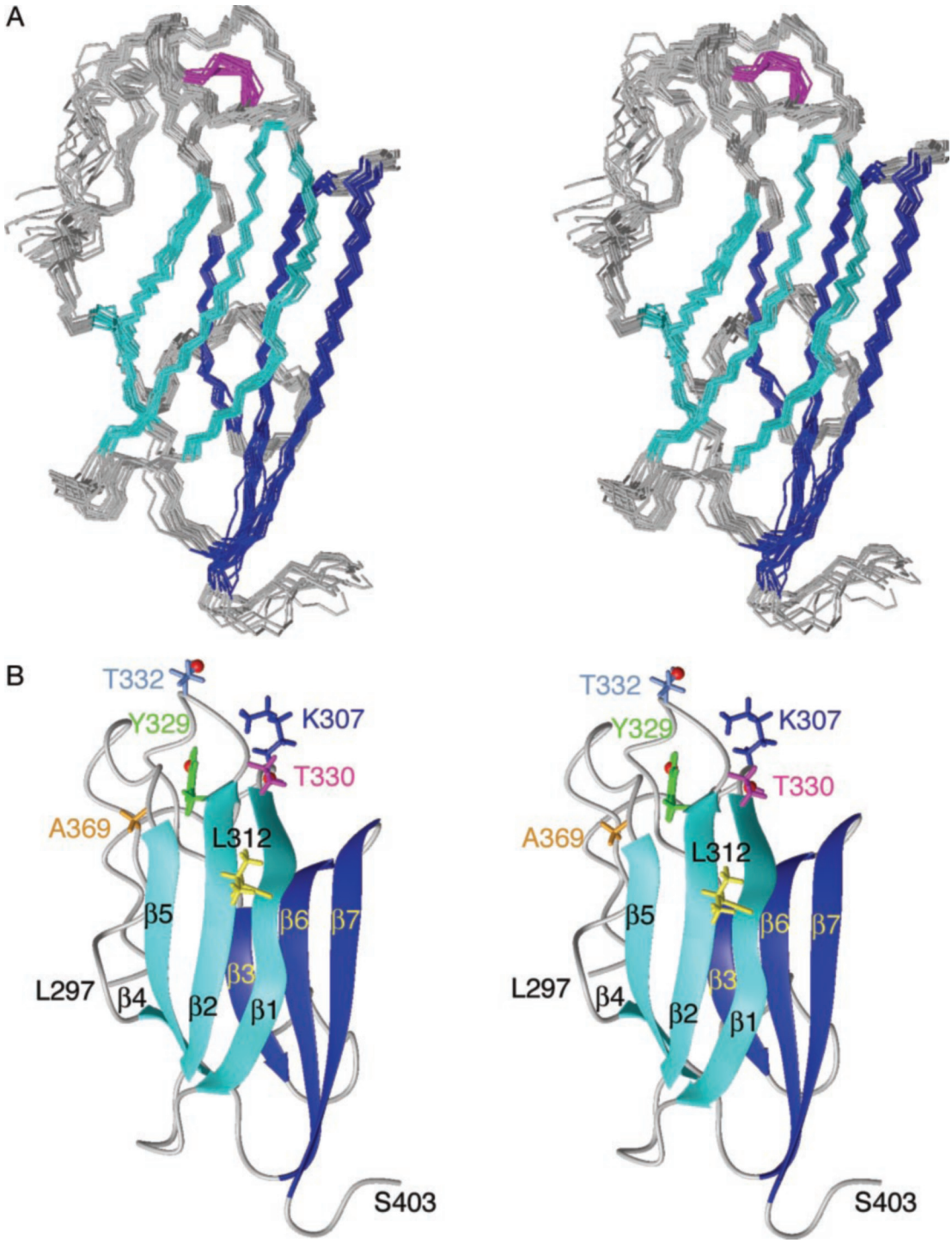

FIG. 1. **The solution structure of WN-rED3.** *A*, backbone trace of 15 low energy structures shown in stereo. Atoms involved in the disulfide bond between Cys^{305} and Cys^{336} are shown in *magenta* near the *top* of the figure. *B*, ribbon diagram of WNV-I domain III. The side chains of several amino acids important for antigenic differences between WNV strains are also shown.

was consistent with the greater neutralizing activity of this Mab against WNV NY99 (Fig. 2, Table II).

Neutralization escape variants selected with MAbs 5C5 (designated Mab^R-5C5) or 5H10 (MAb^R-5H10) encoded mutations at K307R or T330I, respectively (9). When mapped onto the DEN2 E protein dimer structure, the WNV E-D3 NMR structure clearly shows that these residues are surface-exposed and located spatially near to each other on the upper outside face of E-D3 (Fig. 3*B*). To better quantify the effects of these mutations on the epitopes recognized by the anti-WNV MAbs, the ability of all four MAbs to bind to recombinant E-D3 proteins that encoded the K307R or T330I mutations was assessed. Despite the close proximity of residues 307 and 330 on the E-D3 surface (Fig. 1), significantly different mutation effects were observed in the binding of the four MAbs (Fig. 2*B*). The maximal binding of MAb 7H2 (at 100 nM concentration) to either mutant protein was ~2-fold lower than its binding to the wild-type WNV NY99 ED3. In contrast, either mutation resulted in ~5–10-fold reductions in the binding of either the 5H10 or 3A3 MAbs to levels that were only slightly higher than the background. The binding of MAb 5C5 was affected differently by the two mutations. At concentrations up to and including 100 nM, binding to

TABLE I
Summary of structure constraints and statistics

Total restraints	1859
NOE restraints	1239
Intra-residue	299
Sequential	433
Medium range	104
Long range	403
TALOS ϕ/ψ dihedral angles	192
Hydrogen bonds	41
Chiral/ω angle restraints	387
Structural statistics	
NOE violations >0.3 Å	6 ± 2
Dihedral angle violations[a] >20°	8 ± 1
r.m.s.d. from ideal geometry	
Bond lengths (Å)	0.013
Bond angles (°)	2.2
Restraint error r.m.s.d.	
Distance restraints (Å)	0.0156 ± 0.0017
Angular restraints (°)	1.60 ± 0.06
Atomic r.m.s.d. for residues 13–108	
Backbone atoms (Å)[b]	0.65 ± 0.12
All heavy atoms (Å)[b]	0.98 ± 0.17
Ramachandran statistics	
Most favored regions (%)	76.8
Additionally allowed (%)	21.2
Generously allowed (%)	0.7
Disallowed (%)	1.2

[a] A 20°-limit for restraint errors was used due to the small error bars used on the TALOS derived distance restraints, which were as small as ±3° and were less than ±20° for 75% of the dihedral restraints.
[b] Calculated for residues 13–108.

the K307R protein was not detected, whereas only an ~2-fold reduction in peak binding occurred with the T330I mutant. In general, the binding data were consistent with neutralization data obtained for the four MAbs against the MAb^R-5C5 and -5H10 variant strains (Table II). The data also confirmed our previous hypothesis that distinctly different binding interactions can occur at this surface despite the relatively small E-D3 surface area available for antibody binding.

NMR studies of the binding of a JEV-specific neutralizing MAb binding to JEV E-D3 have indicated that multiple interactions occur with residues across the entire upper surface of E-D3 (13). However, escape from neutralization by that JEV-specific MAb was primarily associated with mutations at the outside edge of E-D3 in the β2-β3 loop (15). This region is homologous to the location of the antigenically significant mutations that we have reported in WNV (9). In JEV-rED3, the positively charged K307 of WN-rED3 is replaced by a negatively charged glutamic acid, and residues T330 and T332 are replaced by serines. This suggests that the upper edge of domain III formed by the loop linking β2 and β3 represents an important antigenic determinant for both WNV and JEV. The fact that none of these mutations have been associated with viability or virulence changes in either JEV (15) or WNV (9) suggests that other surface-exposed residues in E-D3 may represent critical receptor binding elements and determinants of tropism and virulence for these viruses.

DISCUSSION

The solution structure of domain III from the envelope protein of the West Nile virus represents the first high-resolution structure from the immunogenically important E protein of this medically important virus. The structure is similar to the domain III structures of both the DEN2V and the JEV but has significant differences that most likely contribute to the antigenic and tropism differences between these mosquito-borne flaviviruses. A number of E-D3 residues in WNV lineage 1 strains that are different from those in some WNV lineage 2 strains, JEV, and/or DEN2V strains are located near the top of the β-barrel (Fig. 1*B*). Among them are Lys^{307} and Thr^{330},

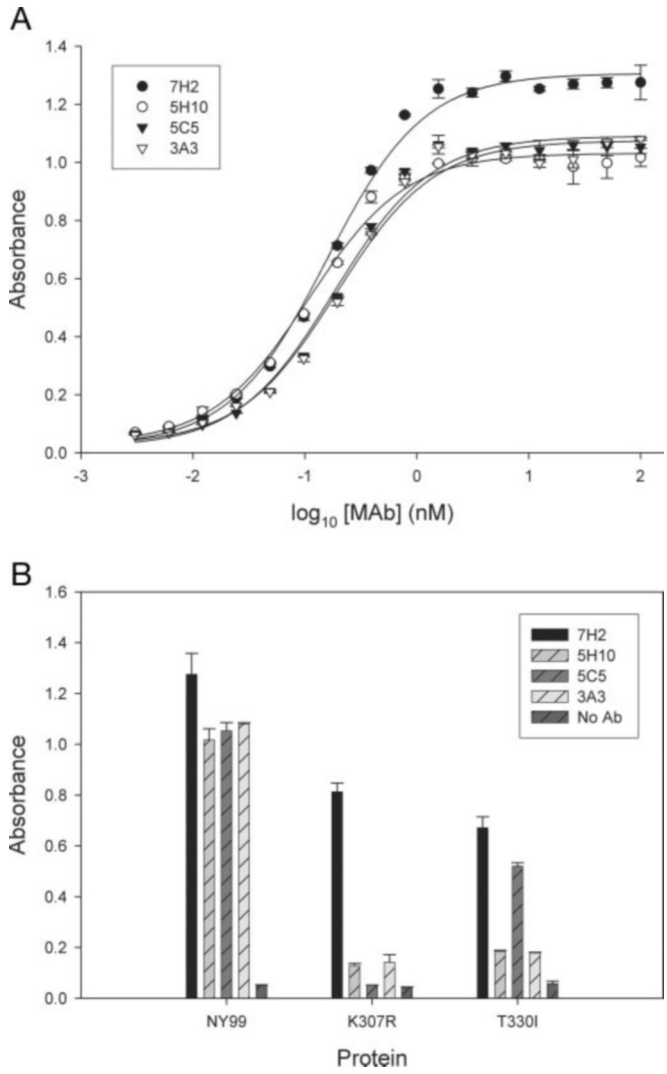

FIG. 2. *A*, binding of WNV-specific neutralizing monoclonal antibodies (7H2, 5H10, 5C5, and 3A3) to WN-rED3. *B*, binding of monoclonal antibodies at 100 nM concentration to either WN-rED3 or its mutants K307R and T330I.

TABLE II
Neutralization of wild-type NY99 or neutralization escape variants by anti-domain III monoclonal antibodies at 10 nM concentration

Virus strain	Neutralization index[a] for MAb			
	7H2	5H10	5C5	3A3
NY99	3.7	2.8	2.6	2.7
MAb^R-5C5 (K307R)	2.7	0.3	0.0	0.1
MAb^R-5H10 (T330I)	2.6	0.8	2.3	0.6

[a] Neutralization index is $\log_{10}$ reduction in virus titer in the presence of MAb compared with a "No MAb" control.

which affect antibody binding and escape from neutralization (see below). In addition, residues Thr^{332}, Tyr^{329}, Leu^{312}, and Ala^{369} are also solvent-exposed, may play a role in the determination of antigenic specificities, and serve as additional starting points for mutation studies.

Comparison with Domains III of the Dengue-2 and Japanese Encephalitis Virus E Proteins—Although the WN-rED3 structure is similar to domain III from both DEN2V (6) and the JEV (JEV-rED3) (13) E proteins, there are significant differences. When aligning the backbone atoms of the six major β-strands present in domain III of all three proteins, WN-rED3 has an atomic r.m.s.d. of 2.5 and 2.8 Å *versus* the domain III of DEN2V and JEV, respectively. Small differences do exist between the

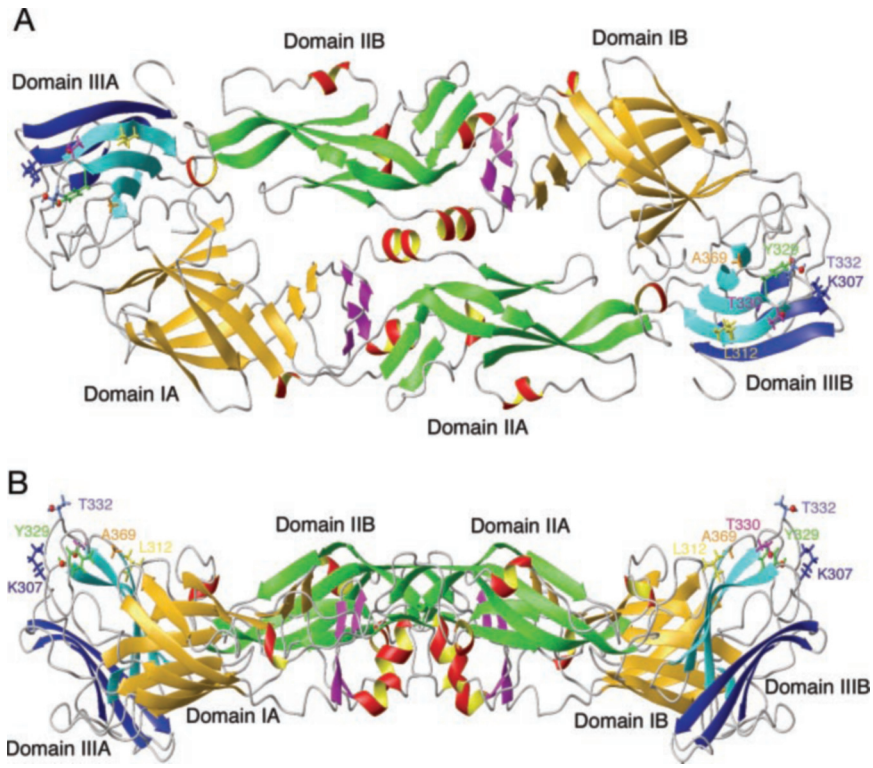

FIG. 3. **Structure of WN-rED3 domain III modeled onto the dengue-2 virus E protein dimer.** *A*, as viewed from the virion surface. *B*, the same structure viewed after rotating the top of the model 90° toward the viewer. Side chain atoms are shown for some residues that have been shown to differentiate antibody binding between West Nile virus strains I and II.

TABLE III
Comparison of β-strands in domain III of the envelope proteins from the dengue-2, West Nile, and Japanese encephalitis viruses

DEN2V		WNV		JEV	
β-strand	Residues	β-strand	Residues	β-strand	Residues
β1	Phe^{306}–Glu^{314}	β1	Phe^{309}–Asp^{317}	β1	Phe^{308}–Asp^{316}
β2	Ile^{320}–Tyr^{326}	β2	Val^{323}–Tyr^{329}	β2	Val^{322}–Tyr^{328}
β3	Cys^{333}–Lys^{339}				
β4	Phe^{337}–Mel^{340}	β3	Ile^{340}–Val^{348}	β3	Ile^{339}–Ala^{343}
β5	Val^{397}–Leu^{351}	β4	Arg^{359}–Leu^{355}		
β6	Ile^{357}–Val^{359}				
β7	Val^{365}–Glu^{370}	β5	Lys^{370}–Glu^{376}	β4	Lys^{369}–Met^{374}
β8	Gly^{374}–Ile^{380}	β6	Gly^{380}–Arg^{388}	β5	Ser^{381}–Gly^{386}
β9	Leu^{387}–Lys^{393}	β7	Gln^{391}–Lys^{399}	β6	Gln^{391}–Trp^{396}

sheet structures of the three proteins (Table III). The first two β-strands of WN-rED3, spanning Phe^{309}–Asp^{317} and Val^{323}–Tyr^{329}, are identical in length to strands β1 and β2 in the both the JE-rED3 and the DEN2 domain III structures. Strand β3 of WN-rED3, spanning Ile^{340}–Val^{343}, is one residue shorter on the C-terminal end compared with the analogous strands β3 (Ile^{339}–Ale^{343}) in JE-rED3 and β4 (Phe^{337}–Met^{340}) in DEN2V. The two-residue strand β4 of WN-rED3 (Arg^{354}–Leu^{355}) coincides with the last two residues of the DEN2 twisted β-strand β5 (Val^{347}–Leu^{351}). The β5 strand of DEN2V appears to be two sequential β-strands that are three and two residues long, twisted ~90° relative to each other. An analogous β-strand is not present in the JE-rED3 structure. Strand β5 (Lys^{370}–Glu^{376}) of WN-rED3 is one residue longer than β4 of JE-rED3 (Lys^{369}–Met^{374}) on the C-terminal end, and it is one residue longer than β7 (Val^{365}–Glu^{370}) of DEN2 on the N-terminal end. β-Strands β6 (Gly^{380}–Arg^{388}) and β7 (Gln^{391}–Lys^{399}) of WN-rED3 are each two residues longer than the analogous strands, β8 (Gly^{374}–Ile^{380}) and β9 (Leu^{387}–Lys^{393}), in DEN2V. The analogous strands β5 (Ser^{381}–Gly^{386}) and β6 (Gln^{391}–Trp^{396}) in JE-rED3 are each one residue shorter than those of the DEN2V and three residues shorter than those of WN-rED3. Two short interacting β-strands that are present in DEN2V domain III, β3 (Cys^{333}–Lys^{334}) and β6 (Ile^{357}–Val^{358}), are not observed in either the WN-rED3 or JE-rED3 solution structures. The two β-strands not present in the JEV and WNV domain III solution structures are near the top of the DEN2V β-barrel. As previously suggested (13), the absence of these two strands may be because of the lack of dimeric head-to-tail interactions between domain III and domains I and II, which are not part of the present protein studied or the JEV domain III solution structure.

Although the secondary structures and global folds of the West Nile, Japanese encephalitis, and dengue-2 virus domain III proteins are similar, the protein surfaces presented as antigens or targets for potential therapeutic drugs are significantly different (Fig. 4). Domain III forms a pentameric pore in the virion, and the residues near this interface are shown in Fig. 4, at the *top*. For WN-rED3, residues Thr^{332}, Ala^{365}, Thr^{366}, and Asn^{368} form a small pocket at this site. The width of the pocket between residues Thr^{332} and Thr^{366} is 6.85 Å. A similar but wider pocket is present in the JEV-rED3 structure. In the JEV-rED3 structure, the pocket is formed by residues Ser^{330}, Asp^{331}, Pro^{333}, Ser^{363}, Ser^{364}, and Asn^{366}. The width across the pocket between residues $Ser^{330}$and Ser^{364}, which are analogous to Thr^{332} and Thr^{366} in WN-rED3, is 8.95 Å. Thus, in the West Nile virus, this pocket is about 2 Å narrower. In addition, the pocket in the JEV-rED3 structure involves more residues, including the negatively charged Asp^{331}. In the West

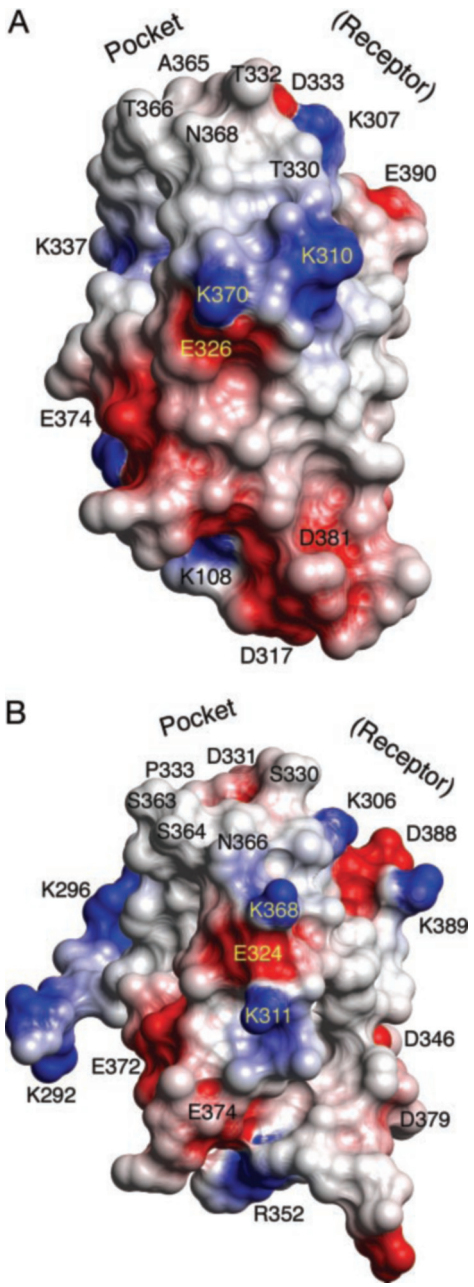

FIG. 4. **Electrostatic contour maps of the WN-rED3 (*A*) and JEV-rED3 (*B*) proteins.** The putative receptor-binding sites of the proteins are located at the *top right* of each panel. Small electroneutral pockets, containing solvent-exposed threonines or serines, are located at the *top* of each protein.

Nile structure, the side chain of the analogous residue Asp^{333} is situated away from this pocket.

The electrostatic charges are also significantly different near these pockets and on the face of the proteins. The electrostatic surface formed in WN-rED3 by residue Lys^{307} sandwiched between two negatively charged residues, Asp^{333} and Glu^{390} (Fig. 4*A*, *top right*), is very different from that formed by JEV-rED3 (Fig. 4*B*, *top right*). In the JEV-rED3 structure, the negatively charged residue Asp^{388} is situated between two positive residues, Lys^{306} and Lys^{389}.

On the central face of the structures shown in Fig. 4, Asp^{326} and Lys^{370} of WN-rED3 align well with residues Glu^{324} and Lys^{368} of JE-rED3. However, in the WN-rED3 structure an additional positively charged residue, Lys^{310}, is just above and to the right of these residues, whereas in the JEV-rED3 structure an additional positively charged residue, Lys^{311}, is directly under the aforementioned residues. These subtle structural changes are responsible for protein surfaces that interact differently with ligands such as antibodies, potential drugs, and possibly cell surface proteins. As an example, the rings of positive lysines in each of the proteins, such as Lys^{307}, Lys^{310}, Lys^{370}, and Lys^{337} in WN-rED3, serve as attractive targets for nucleic acid-based aptamer strategies. Thus, the WN-rED3 structure provides direction for future drug development and mutation effect studies and provides insight in the analysis of current mutation studies.

Antibody neutralization experiments indicate mutations K307R and T330I have differential effects with respect to the antibody used in the experiment. At 100 nM concentration, which is 50–100-fold greater than the K_d for binding of each MAb to wild-type NY99 rE-D3, an ~2-fold reduction in binding was observed for MAb 7H2 to either the K307R or T330I mutants, relative to the NY99 protein. MAbs 5H10 and 3A3 exhibited a 5–10-fold reduction in binding to either of the mutants. However, MAb 5C5 binding was decreased >10-fold to the K307R mutant but was decreased only 2-fold to the T330I mutant. These differences in binding correlated with differences in the ability of these MAbs to neutralize WNV strains encoding those mutations and confirmed that, despite the relatively small size of E-D3, distinctly different binding interactions can occur at its upper surface. In addition, the clustering of antigenically significant mutations at the upper outside edge of E-D3 in both WNV and JEV suggest that other surface-exposed residues may represent critical receptor binding determinants. Accordingly, these solvent-exposed residues represent potentially important targets for rational design of vaccines or therapeutic agents to control WNV disease.

This high-resolution structure of the WN-rED3 provides significant insight toward understanding the immunological differences between a mosquito-borne flavivirus, in general, and members of the JEV serocomplex, more specifically. These subtle structural differences, particularly in areas that constitute virus-specific neutralizing epitopes, may provide the basis for the lack of significant immunological cross-protection between viruses such as WNV, JEV, and DEN2V, despite the antigenic cross-reactivity that exists between them. The structural differences and variability of surface exposed residues of the putative receptor-binding domain III may also contribute to differences in host cell tropism and to subsequent disease pathogenesis of a particular flavivirus (*e.g.* neurotropic WNV and JEV *versus* DEN). The identification of conserved and variable structures and surface residues provides potential targets for the development of structure-based antiviral agents that are targeted against WNV infection, or potentially, infection by all flaviviruses.

Acknowledgment—We thank Bo Xu and coworkers of the University of Texas Medical Branch Protein Expression Core Facility for the expression and purification of WN-rEd3.

REFERENCES

1. Zeller, H. G., and Schuffenecker, I. (2004) *Eur. J. Clin. Microbiol. Infect. Dis.* **23**, 147–156
2. Estrada-Franco, J. G., Navarro-Lopez, R., Beasley, D.W.C., Coffey, L., Carrara, A.-S., Travassos da Rosa, A., Clements, T., Wang, E., Ludwig, G. V., Cortes, A. C., Ramirez, P. P., Tesh, R. B., Barrett, A. D., and Weaver, S. C. (2003) *Emerg. Infect. Dis.* **9,** 1604–1607
3. Blitvich, B. J., Fernandez-Salas, I., Contreras-Cordero, J. F., Marlenee, N. L., Gonzalez-Rojas, J. I., Komar, N., Gubler, D. J., Calisher, C. H., and Beaty, B. J. (2003) *Emerg. Infect. Dis.* **9,** 853–856
4. Loroño-Pino M.A., Blitvich, B. J., Farfán-Ale, J. A., Puerto, F. I., Blanco, J. M., Marlenee, N. L., Rosado-Paredes, E. P., Garcia-Rejon, J. E., Gubler, D. J., Calisher, C. H., and Beaty, B. J. (2003) *Emerg. Infect. Dis.* **9,** 857–859
5. Rey, F. A., Heinz, F. X., Mandl, C., Kunz, C., and Harrison, S. C. (1995) *Nature* **375,** 291–298
6. Modis, Y., Ogata, S., Clements, D., and Harrison, S. C. (2003) *Proc. Natl. Acad. Sci. U. S. A.* **100,** 6986–6991

7. Mandl, C. W., Guirakhoo, F., Holzmann, H., Heinz, F. X., and Kunz, C. (1989) *J. Virol.* **63,** 564–571
8. Hung, J.-J., Hsieh, M.-T., Young, M.-J., Kao, C.-L., King, C.-C., and Chang, W. (2004) *J. Virol.* **78,** 378–388
9. Beasley, D. W. C., and Barrett, A. D. T. (2002) *J. Virol.* **76,** 13097–13100
10. Kuhn, R. J., Zhang, W., Rossman, M. G., Pletnev, S. V., Corver, J., Lenches, E., Jones, C. T., Mukhopadhyay, S., Chipman, P. R., Strauss, E. G., Baker, T. S., and Strauss, J. H. (2002) *Cell* **108,** 717–725
11. Mukhopadhyay, S., Kim, B. S., Chipman, P. R., Rossmann, M. G., and Kuhn, R. J. (2003) *Science* **302,** 248
12. Modis, Y., Ogata, S., Clements, D., and Harrison, S. C. (2004) *Nature* **427,** 313–319
13. Wu, K.-P., Wu, C.-W., Tsao, Y.-P., Kuo, T.-W., Lou, Y.-C., Lin, C.-W., Wu, S.-C., and Cheng, J.-W. (2003) *J. Biol. Chem.* **278,** 46007–46013
14. Laskowski, R. A., Rullman, J. A. C, MacArthur, M. W., Kaptein, R., and Thornton, J. M. (1996) *J. Biomol. NMR* **8,** 477–496
15. Lin, C. W., and Wu, S. C. (2003) *J. Virol.* **77,** 2600–2606
16. Sattler, M., Schleucher, J., and Griesinger, C. (1999) *Prog. NMR Spectrosc.* **34,** 93–158
17. Ikura, M., Bax, A., Clore, G. M., and Gronenborn, A. M. (1990) *J. Am. Chem. Soc.* **112,** 9020–9022
18. Marion, D., Kay, L. E., Sparks, S. W., Torchia, D. A., and Bax, A. (1989) *J. Am. Chem. Soc.* **111,** 1515–1517
19. Clore, G. M., and Gronenborn, A. M. (1994) *Methods Enzymol.* **239,** 249–363
20. Vuister, G. W., and Bax, A. (1992) *J. Magn. Reson.* **98,** 428–435
21. Duggan, B. M., Legge, G. B., Dyson, H. J., and Wright, P. E. (2001) *J. Biomol. NMR* **19,** 321–329
22. Cornilescu, G., Delaglio, F., and Bax, A. (1999) *J. Biomol. NMR* **13,** 289–302
23. Case, D. A., Pearlman, D. A., Caldwell, J. W., Cheatham, T. E., III, Rose, W. S., Simmerling, C. L., Darden, K. M., Merz, R. V., Stanton, A. L., Cheng, J. J., Vincent, M., Crowley, D. M., Ferguson, R. J., Radmer, G. L., Seibel, U. C., Singh, P. K., Weiner, S. J., and Kollman, P. A. (1999) *AMBER6,* University of California, San Francisco, CA
24. Koradi, R., Billeter, M., and Wuthrich, K. (1996) *J Mol. Graphics* **14,** 51–55
25. Volk, D. E., Kallick, D. A., Holbrook, M. R., Beasley, D. W. C., Barrett, A. D. T., and Gorenstein, D. G. (2004) *J. Biomol. NMR* **29**, 399–402